https://doi.org/10.5194/gmd-2020-431
Preprint. Discussion started: 4 March 2021

Geoscientific Model Development Discussions

Sensitivity of asymmetric Oxygen Minimum Zones to remineralization rate and mixing intensity in the tropical Pacific using a basin-scale model (OGCM-DMEC V1.2)

Kai Wang[1], Xiujun Wang[1,2*], Raghu Murtugudde[2], Dongxiao Zhang[3], Rong-Hua Zhang[4]

[1]College of Global Change and Earth System Science, Beijing Normal University, Beijing 100875, China
[2]Earth System Science Interdisciplinary Center, University of Maryland, College Park, Maryland 20740, USA
[3]JISAO, University of Washington and NOAA, Pacific Marine Environmental Laboratory, Seattle, Washington 98115, USA
[4]Institute of Oceanology, Chinese Academy of Sciences, Qingdao, Shandong 266071, China

Correspondence to: Xiujun Wang (xwang@bnu.edu.cn)

Abstract. The tropical Pacific Ocean holds the world's two largest Oxygen Minimum Zones (OMZs), showing a prominent hemispheric asymmetry, with a much stronger and broader OMZ north of the equator. However, many models have difficulties in reproducing the observed asymmetric OMZs in the tropical Pacific. Here, we apply a fully coupled basin-scale model (OGCM-DMEC V1.2) to evaluate the impacts of remineralization rate and the intensity of vertical mixing on the dynamics of OMZs in the tropical Pacific. We first utilize observational data of dissolved oxygen (DO), dissolved organic nitrogen (DON) and oxygen consumption to calibrate and validate the basin-scale model. Our model experiments demonstrate that enhanced vertical mixing combined with reduced remineralization rate can significantly improve our model capability of reproducing the asymmetric OMZs. Our study shows that DO is more sensitive to biological processes over 200-400 m but to physical processes over 400-1000 m. Enhanced vertical mixing not only causes an increase in DO supply at mid-depth, but also results in lower rates of biological consumption in the OMZs, which is associated with redistribution of DON. Our analyses demonstrate that weaker physical supply in the ETNP is the dominant process responsible for the asymmetry of the lower OMZs whereas greater biological consumption to the north plays a larger role in regulating the upper OMZs. This study highlights the complex roles of physical supply and biological consumption in shaping the asymmetric OMZs in the tropical Pacific.

1 Introduction

Photosynthesis and respiration are important processes in all ecosystems on the Earth, with carbon and oxygen being the two main elements. The carbon cycle has garnered much attentions, which made significant progresses in both the observations and modelling of biological processes (e.g., uptake of CO_2 and respiration), and physical/chemical processes (e.g., carbon fluxes between the atmosphere, land and ocean). However, the oxygen cycle has received much less attention despite its large role in the earth system (Breitburg *et al.*, 2018; Oschlies *et al.*, 2018).

https://doi.org/10.5194/gmd-2020-431
Preprint. Discussion started: 4 March 2021


Geoscientific Model Development Discussions

Dissolved oxygen (DO) is a sensitive indicator of physical and biogeochemical processes in the ocean thus a key parameter for understanding the ocean's role in the climate system (Stramma *et al.*, 2010). In addition to photosynthesis and respiration, the distribution of DO in the world's oceans is also regulated by air-sea gas exchange, ocean circulation and ventilation (Bopp *et al.*, 2002; Bettencourt *et al.*, 2015; Levin, 2018). Unlike most dissolved nutrients that display an increase in concentration with depth, DO concentration is generally low at mid-depth of the ocean. The most remarkable feature in the oceanic oxygen dynamics is the so-called Oxygen Minimum Zone (OMZ) that is often present below 200 m in the open oceans (Karstensen *et al.*, 2008; Stramma *et al.*, 2008).

The world's two largest OMZs are observed in the Eastern Tropical North Pacific (ETNP) and South Pacific (ETSP), showing a peculiar asymmetric structure across the equator, i.e., a much larger volume of suboxic water (<20 mmol m^{-3}) to the north than to the south (Paulmier and Ruiz-Pino, 2009; Bettencourt *et al.*, 2015). It is known that OMZs are caused by the biological consumption associated with remineralization of organic matter (OM), and weak physical supply of DO due to sluggish subsurface ocean circulation and ventilation (Czeschel *et al.*, 2011; Brandt *et al.*, 2015; Kalvelage *et al.*, 2015). Although there have been a number of observation based analyses addressing the dynamics of OMZs in the tropical Pacific during the past decade (Stramma *et al.*, 2010; Czeschel *et al.*, 2012; Schmidtko *et al.*, 2017; Garçon *et al.*, 2019), our understanding is uncompleted in terms of the underlying mechanisms that regulate DO dynamics at mid-depth due to the limitation of available data (Stramma *et al.*, 2012; Oschlies *et al.*, 2018).

Large-scale physical-biogeochemical models have become a useful tool to investigate the potential sensitivity of OMZs to climate change (Duteil and Oschlies, 2011; Williams *et al.*, 2014; Ward *et al.*, 2018). However, many models still have some difficulties in reproducing observed asymmetric OMZs in the tropical Pacific (Cabre *et al.*, 2015; Shigemitsu *et al.*, 2017), which may be due to "unresolved ocean transport processes, unaccounted for variations in respiratory oxygen demand, or missing biogeochemical feedbacks" (Oschlies *et al.*, 2018). A common problem is that the two asymmetric OMZs merge into one in most models that often overestimate the volume of OMZs in the tropical Pacific, which may be related to weaker physical supply and/or higher rates of biological consumption (Cabre *et al.*, 2015; Shigemitsu *et al.*, 2017). Recent studies have also indicated that a realistic representation of circulation and ventilation processes with a high-resolution ocean model is critical to predict the asymmetric OMZs in the tropical Pacific (Berthet *et al.*, 2019; Busecke *et al.*, 2019). Apparently, it's necessary to carry out model-data integrative studies to improve model capacity of simulating the dynamics of the tropical OMZs, and to better understand the relative roles of physical and biological processes.

A basin-scale ocean general circulation model coupled with a dynamic marine ecosystem-carbon model (OGCM-DMEC) was developed for the tropical Pacific (Wang *et al.*, 2008; Wang *et al.*, 2009b; Wang *et al.*, 2015), which showed capability of reproducing observed spatial and temporal variations of physical, nutrient and carbon fields in the upper ocean. In this study, we conduct model sensitivity experiments and evaluation on responses of mid-depth DO to parameterizations of two

https://doi.org/10.5194/gmd-2020-431
Preprint. Discussion started: 4 March 2021


Geoscientific Model Development Discussions

relevant processes (i.e., remineralization and vertical mixing). We first carry out model calibration and validation using observational data of DO and consumption rate to improve the simulation of OMZs in the tropical Pacific. Then, we use the improved model to evaluate how biological consumption and physical supply regulate the dynamics of mid-depth DO. The objective of this study is to advance our model capacity to simulate the oceanic oxygen cycle, and to identify the mechanisms driving the asymmetric OMZs in the tropical Pacific.

2. Model description

2.1 Ocean physical model

The basin-scale OGCM, a reduced-gravity, primitive-equation, sigma-coordinate model, is coupled to an advective atmospheric model (Murtugudde *et al.*, 1996). There are 20 layers with variable thicknesses in the OGCM. The mixed layer (the upper-most layer) depth is determined by the Chen mixing scheme (Chen *et al.*, 1994), which varies from 10 m to 50 m on the equator. The remaining layers in the euphotic zone are approximately 10 m in thickness. The model domain is between 30ºS and 30ºN, and zonal resolution is 1º. Meridional resolution varies between 0.3º and 0.6º over 15ºS-15ºN (1/3° over 10°S-10ºN), and increases to 2º in the southern and northern "sponge layers" (the 25º-30º bands) where temperature, salinity, and nitrate are gradually relaxed back towards the observed climatological seasonal means from the World Ocean Atlas, 2013 (WOA2013: http://www.nodc.noaa.gov/OC5/woa13/pubwoa13.html).

The model is forced by atmospheric conditions: climatological monthly means of solar radiation and cloudiness, and interannual 6-day means of precipitation and surface wind stress. Precipitation is from ftp://ftp.cdc.noaa.gov/Datasets/gpcp. Wind stresses are from the National Centers for Environmental Prediction (NCEP) reanalysis (Kalnay *et al.*, 1996). Air temperature and humidity above the ocean surface are computed by the atmospheric mixed layer model. Initial conditions were obtained from outputs of an interannual hindcast simulation over 1948-1978, which itself is initialized from a climatological run with a 30-year spin up. The initial conditions for the climatological spin up are specified from the WOA2013. We carry out an interannual simulation for the period of 1978-2018, and analyse model output for the period of 1981-2000.

2.2 Ocean biogeochemical model

The DMEC model is the main part of the biogeochemical model that is embedded in the basin-scale OGCM. The DMEC model consists of eleven components: small (S) and large (L) sizes of phytoplankton (P_S and P_L), zooplankton (Z_S and Z_L) and detritus (D_S and D_L), dissolved organic nitrogen (DON), ammonium, nitrate, dissolved iron, and DO (Figure 1). All biological components use nitrogen as their unit, and are computed in a manner similar to physical variables.

In this model, net community production (NCP) is computed as:

https://doi.org/10.5194/gmd-2020-431
Preprint. Discussion started: 4 March 2021


Geoscientific Model Development Discussions

$$NCP = 6.625(\mu_s P_s + \mu_L P_L - r_s Z_s - r_L Z_L - c_{DON} DON - c_{DS} D_s - c_{DL} D_L) \quad (1)$$

where 6.625 is the C:N ratio, μ the rate of phytoplankton growth, r the rate of zooplankton respiration, c the rates of detritus decomposition and DON remineralization. The equations for biogeochemical processes and model parameters are described in Appendix A and B. There have been changes in some parameters comparing with those in Wang *et al.* (2008), which were based on our model calibration and validation for chlorophyll (Wang *et al.*, 2009a), nitrogen cycle (Wang *et al.*, 2009b) and carbon cycle (Wang *et al.*, 2015).

2.3 Computation of oxygen sources and sinks

The time evolution of DO is regulated by physical, biological and chemical processes:

$$\frac{\partial O_2}{\partial t} = -u\frac{\partial O_2}{\partial x} - v\frac{\partial O_2}{\partial y} - w\frac{\partial O_2}{\partial z} + O_{mix} - O_{bio} + O_{gas} \quad (2)$$

where u, v, and w are zonal, meridional, and vertical velocity, respectively. O_{mix} is the vertical mixing term that is calculated by three subroutines. Briefly, the first one computes convection to remove instabilities in the water column, and the second one determines the mixed layer depth. The third one computes partial vertical mixing (K_z) between two adjacent layers to relieve gradient Richardson (R_i) number instability, which is calculated as follows:

$$K_z = \left(1 - \left(\frac{Ri}{0.7}\right)^{\lambda}\right) (Ri < 0.7) \quad (3)$$

$$K_z = 0 \ (Ri \geq 0.7) \quad (4)$$

where the mixing parameter λ is set to 1.

The biological source/sink term O_{bio} is computed as follows:

$$O_{bio} = 1.3\text{NCP} \quad (5)$$

where 1.3 is the O:C Redfield ratio. Below the euphotic zone, DO concentration is determined by physical supply and biological consumption that results from detritus decomposition and DON remineralization, in which DON remineralization is dominant because DON poor is several times greater than detritus (Wang *et al.*, 2008).

The flux of O_2 from the atmosphere to the surface ocean is computed as:

$$O_{gas} = (O_{Sat} - O)K_0 \quad (6)$$

where O_{sat} is the O_2 saturation, a function of temperature and salinity (Weiss, 1970), and K_0 the gas transfer velocity that is a function of wind speed (u_s) and SST according to Wanninkhof (1992):

$$K_0 = 0.31 u_s^2 \sqrt{\frac{Sc}{Sc20}} \quad (7)$$

where Sc and Sc_{20} are the Schmidt number at SST and 20° C, respectively:

$$S_c = 1953 - 128T + 3.99T^2 - 0.05T^3 \quad (8)$$

https://doi.org/10.5194/gmd-2020-431
Preprint. Discussion started: 4 March 2021


Geoscientific Model Development Discussions

3. Model experiments and validation

3.1 Evaluation of DO distribution from the reference run

We first evaluate simulated DO for the tropical Pacific Ocean using the outputs from OGCM-DMEC V1.2 (hereafter reference run). We focus on model-data comparisons over 200-400 m, 400-700 m and 700-1000 m that broadly represent the upper OMZ, lower OMZ and beneath OMZ, respectively. The WOA2013 data shows a much larger area of suboxic waters (<20 mmol m^{-3}) in the ETNP than in the ETSP over 200-400 m and 400-700 m (Figure 2a and 2c), but no suboxic water over 700-1000 m (Figure 2e). Although the reference run produces two OMZs off the equator over 200-400 m (Figure 2b), the sizes of suboxic water are much larger in the reference run than those in the WOA2013 data. The reference run significantly over-estimate the size of suboxic water and underestimates DO concentration over 400-700 m (Figure 2d). The difference between WOA2013 and the reference run is small over 700-1000 m, except in the eastern tropical Pacific (Figure 2f). The relative roles of the physics vs. the biogeochemistry in determining the bias are diagnosed further below.

3.2 Sensitivity experiments

Given that the mid-depth DO concentration is influenced by physical supply and biological consumption, and remineralization of DON is the dominant process for oxygen consumption, the underestimated DO at mid-depth would be a result of overestimation of consumption associated with DON remineralization and/or underestimation of supply. Indeed, the reference run over-estimates biological consumption over 100-400 m (Figure 3). Thus, we apply a reduced DON remineralization constant (50% of the reference run), which leads to a remarkable improvement in simulated DON and consumption. The reference run applies a zero value for background diffusion. However, a previous modelling study has demonstrated that vertical background diffusion is an important process for DO supply at mid-depth (Duteil and Oschlies, 2011). Accordingly, we conduct a few more simulations (Table 1) to investigate how reducing remineralization rate and applying different values for vertical background diffusion (Kb = 0.1, 0.3, or 0.5 cm^2 s^{-1}) affect simulated DO distribution and asymmetric OMZs in the tropical Pacific. Changing the intensity of vertical diffusion has relatively small influence on vertical distributions of DON and DO consumption in the OMZ (Figure 3).

We then compare simulated DO and WOA2013 climatology data. Figure 4a illustrates a larger volume of suboxic water located north of ~5°N and a smaller volume of suboxic water over 12°S-4°S, which are separated by relatively higher DO (>30 mmol m^{-3}) along the equator. Both Cd0.5 run (Figure 4c) and the reference run (Figure 4b) produce much larger volumes of suboxic water that are extend to the equatorial region, and even merge into one. Clearly, there is an improvement in simulated DO with vertical background diffusion (Figure 4d, 4e and 4f). Overall, Cd0.5Kb0.5 is able to capture the observed spatial distribution of DO, especially the asymmetric feature (i.e., a larger volume of suboxic water to the north but a smaller size of suboxic water to the south), and relatively higher DO (~30-40 mmol m^{-3}) over 2°S-2°N.

https://doi.org/10.5194/gmd-2020-431
Preprint. Discussion started: 4 March 2021


Geoscientific Model Development Discussions

3.3 Model validation

To further evaluate the performance of experiments, three statistical measures are applied over 200-400 m, 400-700 m and 700-1000 m in the ETNP (165°W-90°W, 5°-20°N) and ETSP (110°W-80°W, 10°S-3°S). As shown in Table 2, compared to the reference run, bias, MAE and RMSE all decrease in the new experiments, with the smallest values from Cd0.5Kb0.5 run except over 700-1000 m in the ETNP. For example, both MAE and RMSE are lowest from Cd0.5Kb0.5 run over 200-700 m in the ETNP (6.95-16.44 mmol m^{-3}) and over 200-1000 m in ETSP (3.12-7.59 mmol m^{-3}). Many current models show much large RMSE (~20-80 mmol m^{-3}) with respect to observed DO from mixed layer to 1000 m (Cabre *et al.*, 2015; Bao and Li, 2016). Figure 5 also illustrates that Cd0.5Kb0.5 run produces the best outputs, with the largest correlation coefficients (0.77-0.94) and also the smallest distance to 1 in normalized standard deviation (0.54-1.81 in ETNP and 0.33-1.63 in ETSP).

We also compare the sizes of suboxic water and hypoxic water between model and WOA2013 (Table 3). Based on WOA2013, we estimate that the sizes of suboxic water and hypoxic water are 5.97×10^{15} m^3 and 19.98×10^{15} m^3 in the north, and 1.43×10^{15} m^3 and 7.12×10^{15} m^3 in the south, respectively. While the Cd0.5 run (with a reduced remineralization rate) results in an improvement in simulated OMZ volume, significant improvements are obtained with the combination of reduced remineralization and enhanced vertical mixing (i.e., with background diffusion). Overall, the best performance for reproducing OMZ volume is Cd0.5Kb0.5 simulation that predicts similar volumes for the suboxic water (6.61×10^{15} m^3 to the north and 1.56×10^{15} m^3 to the south) and the hypoxic water (19.62×10^{15} m^3 and 7.13×10^{15} m^3). We then use cruise data to further validate modelled DO from the best run (Cd0.5Kb0.5). Figure 6 shows that the model can generally reproduce the vertical-zonal distribution of DO along 10°N and 17°S, spanning from 1989 to 2009, particularly in the eastern tropical Pacific.

4 Model evaluation and discussions

In this section, we further compare the improved model simulations (Cd0.5 and Cd0.5Kb0.5) with reference run to diagnose the relative contributions of biological consumption and physical supply to the asymmetric OMZs in the tropical Pacific, aiming to identify the underlying mechanisms regulating the dynamics of mid-depth DO.

4.1 Changes of mid-depth DO due to reduced remineralization and enhanced mixing

We first compare the changes of DO concentration between the three model simulation over 200-400 m, 400-700 m, and 700-1000 m (Figure 7). Clearly, reduced remineralization rate largely increase mid-depth DO in all three layers, with a greater increase (~0-22 mmol m^{-3}) over 200-400 m (Figure 7a), a modest increase (~0-6 mmol m^{-3}) over 400-700 m (Figure 7d), and a small increase (0-3 mmol m^{-3}) over 700-1000 m (Figure 7h). Enhanced vertical mixing results in a small increase

https://doi.org/10.5194/gmd-2020-431
Preprint. Discussion started: 4 March 2021


Geoscientific Model Development Discussions

in DO (<10 mmol m^{-3}) over 200-400 m (Figure 7b) but a large increase (5-12 mmol m^{-3}) over 400-700 m and 700-1000 m (Figure 7e and 7i). A number of modelling studies have demonstrated that parameterization of vertical mixing has significant impacts on the mean state of DO distributions at mid-depth (Duteil and Oschlies, 2011; Gnanadesikan *et al.*, 2013).

We also assess the response of mid-depth DO to the combination of reduced remineralization rate and enhanced vertical mixing (Cd0.5Kb0.5 minus reference run). Overall, the increase of DO is greater over 200-400 m (~10-24 mmol m^{-3}) than over 400-700 m (~8-18 mmol m^{-3}) and 700-1000 m (~6-12 mmol m^{-3}) (Figure 7c, 7f & 7j). The spatial pattern and magnitude of increased DO resulted from the combined changes of remineralization rate and vertical mixing have a large similarity to those caused by reduced remineralization rate for the 200-400 m layer (Figure 7a), but are similar to those due to enhanced mixing below 400 m (Figure 7d & 7h). Our analyses indicate that DO dynamics is regulated by biological processes above 400 m, but by physical processes over 400-1000 m. The larger biological influence on the upper OMZ is attributable to the greater rate of DO consumption (Karstensen *et al.*, 2008) whereas the greater physical impact on the lower OMZ reflects the relatively larger role of supply than consumption.

4.2 Responses of consumption and supply to reduced remineralization and enhanced mixing

We then evaluate the changes of biological consumption and physical supply of DO due to reduced remineralization and/or enhanced mixing. Reducing remineralization rate by 50% (Cd0.5 minus reference) leads to large decrease (~1.5-2.0 mmol m^{-3} yr^{-1}) over 200-400 m, modest decrease (~0.2-0.5 mmol m^{-3} yr^{-1}) over 400-700 m and small decrease (~0.1-0.2 mmol m^{-3} yr^{-1}) over 700-1000 m (Figure 8a, 8d and 8h). On the other hand, enhanced vertical mixing causes much greater increase of supply over 400-1000 m than over 200-400 m. Numerous studies have indicated that physical mixing is the only source of DO for the tropical OMZs (Czeschel *et al.*, 2012; Brandt *et al.*, 2015; Talley *et al.*, 2016). For example, turbulent background diffusion accounts for 89% of the net DO supply for the core OMZ layer of south tropical Pacific (Llanillo *et al.*, 2018). Figure 8e and 8i illustrate that physical supply is increased by ~0.2-0.6 mmol m^{-3} yr^{-1} in most of the mid-waters, with the largest increase in the southern part of central equatorial Pacific over 400-700 m. However, there is somehow a small decrease of physical supply in the ETNP over 200-400 m (by ~0.03 mmol m^{-3} yr^{-1}, Figure 8b) and 400-700 m (<0.02 mmol m^{-3} yr^{-1}, Figure 8e), implying that increased DO under enhanced vertical mixing may be attributable to changes in biological consumption.

We further compare biological consumption between Cd0.5Kb0.5 and the Cd0.5. Interestingly, enhanced vertical mixing results in a decrease in consumption, with the largest decreases (~0.03-0.07 mmol m^{-3} yr^{-1}) over 400-700 m (Figure 8f), the smallest decrease (~0.01-0.04 mmol m^{-3} yr^{-1}) over 200-400 m (Figure 8c) and modest decrease of ~0.02-0.04 mmol m^{-3} yr^{-1} over 700-1000 m (Figure 8j). For the northern OMZ, biological consumption decreases by ~0.03-0.07 mmol m^{-3} yr^{-1} over 200-700 m (Figure 8c and 8f), which is larger than the decreased rate (~0.01-0.03 mmol m^{-3} yr^{-1}) of physical supply (Figure 8b and 8e).

https://doi.org/10.5194/gmd-2020-431
Preprint. Discussion started: 4 March 2021


Geoscientific Model Development Discussions

Remineralization rate of DOM in the ocean is determined by the size of DOM pool and temperature (Wang *et al.*, 2008; Brewer and Peltzer, 2016). Given that there is little difference (<10^{-5} °C) in seawater temperature between different model experiments, the reduced consumption rates due to DOM remineralization would be a result of a smaller amount of DOM. Here, we evaluate the zonal and meridional distributions of DON together with remineralization rate. As shown in Figure 9a-9d, modelled consumption decreases from ~8 mmol m^{-3} yr^{-1} in the euphotic zone to ~1-2 mmol m^{-3} yr^{-1} below 400 m, and modelled DON decreases from 5-8 mmol N m^{-3} near the surface to 1-4 mmol N m^{-3} over 400-1000 m. Limited field studies reported that surface DON concentration was ~5-7 mmol N m^{-3} in the ETSP (Loginova *et al.*, 2019), and consumption rate ranged from 8.3 mmol m^{-3} yr^{-1} at ~200 m to <3.1 mmol m^{-3} yr^{-1} below 500 m in the subtropical North Pacific (Sonnerup *et al.*, 2013), which are comparable to our model results. Our model simulations indicate that enhanced vertical mixing leads to a redistribution of DON below 200 m, with a decrease in DON concentration (0.06-0.12 mmol N m^{-3}) over 600-900 m, but an increase (<0.04 mmol N m^{-3}) below 1000 m in the eastern tropical Pacific (Figure 9h, 9i and 9j).

4.3 Impacts of biological consumption and physical supply on asymmetry of OMZs

Previous studies have demonstrated meridional asymmetric features in many physical and biological fields in the tropical Pacific, e.g., temperature and salinity (Fiedler and Talley, 2006), circulation and ventilation (Kessler, 2006; Kuntz and Schrag, 2018), nitrogen and carbon cycles (Libby and Wheeler, 1997; Wang *et al.*, 2009b), which may be largely associated with the asymmetries in water mass exchange between the equatorial and off-equator Pacific Ocean (Kug *et al.*, 2003). Accordingly, one may assume that the hemisphere asymmetry of OMZs could be related to the differences in physical supply and biological consumption between the ETNP and ETSP.

There is evidence that the size of tropical OMZ is largely influenced by biological processes, such as organic matter export and oxygen consumption (Keller *et al.*, 2016; Cavan *et al.*, 2017). Figure 10a illustrates that DO is increased in both ETNP and ETSP over 200-1000 m when remineralization rate decreases by 50%. The increase of DO is generally greater in the ETSP than in ETNP, except in the core OMZ (~300-500 m). Earlier field studies have revealed that DON concentration is much higher to the north than to the south in the central-eastern tropical Pacific (Libby and Wheeler, 1997; Raimbault *et al.*, 1999). Later studies showed that rates of DOM remineralization and/or oxygen consumption are also greater at mid-depth in the ETNP than in the ETSP (Feely *et al.*, 2004; Tiano *et al.*, 2014; Kalvelage *et al.*, 2015), indicating that biological processes play a big role in determining the asymmetry of upper OMZs.

Recent studies also emphasized the role of changes in physical processes for the observed asymmetric OMZs in the tropical oceans. For instance, there is evidence that larger-scale mass transport related to circulation and ventilation in the southern hemisphere is more efficient than in the northern hemisphere (Kuntz and Schrag, 2018), and the transit time from the surface to the OMZ is much longer in the ETNP than in the ETSP (Sonnerup *et al.*, 2013; Fu *et al.*, 2018). Clearly, our model

https://doi.org/10.5194/gmd-2020-431
Preprint. Discussion started: 4 March 2021


Geoscientific Model Development Discussions

experiment shows that enhanced vertical mixing leads to a significant increase in DO concentration below 200 m (Figure 10b). The increase of DO is similar below 1000 m in the ETNP and ETSP, but differs largely between the two regions, with much greater values over 200-1000 m in the ETSP. Our analysis indicates that enhanced vertical mixing increases the physical supply of DO over most of the water column, except over 300-500 m in the ETNP showing a small decrease (Figure 10c). The increase of supply is greater over 200-1000 m in the ETSP than in the ETNP, and significant increases (>0.2 mmol m^{-3} yr^{-1}) are below 600 m (500 m) in the ETNP (ETSP). These analyses indicate that physical transport may be largely responsible for the asymmetry of lower OMZs.

5. Conclusion

This paper describes an evaluation and validation of a fully coupled basin-scale model (OGCM-DMEC V1.2), focusing on the sensitivity of the asymmetric OMZs in the tropical Pacific to different parameterizations of remineralization and vertical mixing. Our results show that the improved model with enhanced vertical mixing combined with reduced remineralization successfully reproduces the observed asymmetric OMZs in the tropical Pacific.

Our results demonstrate that reduced remineralization rate leads to remarkable decrease of biological consumption over 200-400 m, which largely affects the distribution of DO in the upper OMZ. On the other hand, enhanced vertical mixing causes a significant increase in physical supply of DO over 400-1000 m. Apart from the direct impact on physical supply, enhanced vertical mixing also results in the redistribution of DOM in the water column, i.e., an increase over 200-1000 m and a decrease below 1000 m, leading to lower consumption in the OMZs.

Further analyses indicate that the asymmetric OMZs in the tropical Pacific are attributable to the asymmetry in both physical supply and biological consumption. The larger volume of northern OMZ is a result of greater biological consumption and weaker physical supply to the north, in which physical supply plays a dominant role in the lower OMZs but biological consumption also has impacts on the asymmetric DO for the upper OMZs. Future studies utilizing advanced models are needed to better understand the impacts of physical and biological interactions on the variability and drivers of the tropical OMZs.

https://doi.org/10.5194/gmd-2020-431
Preprint. Discussion started: 4 March 2021


Geoscientific Model Development Discussions

Code and data availability. The exact version of the software code used to produce the results presented in this paper is archived on Zenodo (http://doi.org/10.5281/zenodo.4384131, Wang et al., 2020). Other code and data are available upon request from the authors. Request for materials should be addressed to X.J.W. (xwang@bnu.edu.cn).

Author contributions. X.J.W. and K.W. designed the study, performed the simulations and prepared the manuscript. R.M., D.X.Z. and R.H.Z. contributed to analysis, interpretation of results and writing.

Competing interests. The authors declare that they have no conflict of interest.

Acknowledgements. This work was supported by the Chinese Academy of Sciences' Strategic Priority Project (XDA1101010504). The authors wish to acknowledge the use of the Ferret (http://ferret.pmel.noaa.gov/Ferret/).

https://doi.org/10.5194/gmd-2020-431
Preprint. Discussion started: 4 March 2021

Geoscientific Model Development Discussions

References

Bao, Y., Li, Y., 2016. Simulations of dissolved oxygen concentration in CMIP5 Earth system models. Acta Oceanologica Sinica 35, 28-37.

Berthet, S., Séférian, R., Bricaud, C., Chevallier, M., Voldoire, A., Ethé, C., 2019. Evaluation of an Online Grid - Coarsening Algorithm in a Global Eddy - Admitting Ocean Biogeochemical Model. Journal of Advances in Modeling Earth Systems 11, 1759-1783.

Bettencourt, J.H., Lopez, C., Hernandez-Garcia, E., Montes, I., Sudre, J., Dewitte, B., Paulmier, A., Garcon, V., 2015. Boundaries of the Peruvian oxygen minimum zone shaped by coherent mesoscale dynamics. Nature Geoscience 8, 937-U967.

Bopp, L., Le Quere, C., Heimann, M., Manning, A.C., Monfray, P., 2002. Climate-induced oceanic oxygen fluxes: Implications for the contemporary carbon budget. Global Biogeochemical Cycles 16, 1-13.

Brandt, P., Bange, H.W., Banyte, D., Dengler, M., Didwischus, S.H., Fischer, T., Greatbatch, R.J., Hahn, J., Kanzow, T., Karstensen, J., Krortzinger, A., Krahmann, G., Schmidtko, S., Stramma, L., Tanhua, T., Visbeck, M., 2015. On the role of circulation and mixing in the ventilation of oxygen minimum zones with a focus on the eastern tropical North Atlantic. Biogeosciences 12, 489-512.

Breitburg, D., Levin, L.A., Oschlies, A., Gregoire, M., Chavez, F.P., Conley, D.J., Garcon, V., Gilbert, D., Gutierrez, D., Isensee, K., Jacinto, G.S., Limburg, K.E., Montes, I., Naqvi, S.W.A., Pitcher, G.C., Rabalais, N.N., Roman, M.R., Rose, K.A., Seibel, B.A., Telszewski, M., Yasuhara, M., Zhang, J., 2018. Declining oxygen in the global ocean and coastal waters. Science 359.

Brewer, P.G., Peltzer, E.T., 2016. Ocean chemistry, ocean warming, and emerging hypoxia: Commentary. Journal of Geophysical Research: Oceans 121, 3659-3667.

Busecke, J.J.M., Resplandy, L., Dunne, J.P.P., 2019. The Equatorial Undercurrent and the Oxygen Minimum Zone in the Pacific. Geophysical Research Letters, 6716–6725.

Cabre, A., Marinov, I., Bernardello, R., Bianchi, D., 2015. Oxygen minimum zones in the tropical Pacific across CMIP5 models: mean state differences and climate change trends. Biogeosciences 12, 5429-5454.

Cavan, E.L., Trimmer, M., Shelley, F., Sanders, R., 2017. Remineralization of particulate organic carbon in an ocean oxygen minimum zone. Nature communications 8, 14847.

Chen, D., Rothstein, L.M., Busalacchi, A.J., 1994. A Hybrid Vertical Mixing Scheme and Its Application to Tropical Ocean Models. Journal of Physical Oceanography 24, 2156-2179.

Czeschel, R., Stramma, L., Johnson, G.C., 2012. Oxygen decreases and variability in the eastern equatorial Pacific. J Geophys Res-Oceans 117, 1-12.

Czeschel, R., Stramma, L., Schwarzkopf, F.U., Giese, B.S., Funk, A., Karstensen, J., 2011. Middepth circulation of the eastern tropical South Pacific and its link to the oxygen minimum zone. J Geophys Res-Oceans 116.

Duteil, O., Oschlies, A., 2011. Sensitivity of simulated extent and future evolution of marine suboxia to mixing intensity. Geophysical Research Letters 38.

Feely, R.A., Sabine, C.L., Schlitzer, R., Bullister, J.L., Mecking, S., Greeley, D., 2004. Oxygen utilization and organic carbon remineralization in the upper water column of the Pacific Ocean. Journal of Oceanography 60, 45-52.

Fiedler, P.C., Talley, L.D., 2006. Hydrography of the eastern tropical Pacific: A review. Progress in Oceanography 69, 143-180.

Fu, W.W., Bardin, A., Primeau, F., 2018. Tracing ventilation source of tropical pacific oxygen minimum zones with an adjoint global ocean transport model. Deep-Sea Research Part I: Oceanographic Research Papers 139, 95-103.

Garçon, V., Karstensen, J., Palacz, A., Telszewski, M., Aparco Lara, T., Breitburg, D., Chavez, F., Coelho, P., Cornejo-D'Ottone, M., Santos, C., Fiedler, B., Gallo, N.D., Grégoire, M., Gutierrez, D., Hernandez-Ayon, M., Isensee, K., Koslow, T., Levin, L., Marsac, F., Maske, H., Mbaye, B.C., Montes, I., Naqvi, W., Pearlman, J., Pinto, E., Pitcher, G., Pizarro, O., Rose, K., Shenoy, D., Van der Plas, A., Vito, M.R., Weng, K., 2019. Multidisciplinary Observing in the World Ocean's Oxygen Minimum Zone Regions: From Climate to Fish — The VOICE Initiative. Frontiers in Marine Science 6.

Gnanadesikan, A., Bianchi, D., Pradal, M.A., 2013. Critical role for mesoscale eddy diffusion in supplying oxygen to hypoxic ocean waters. Geophysical Research Letters 40, 5194-5198.

https://doi.org/10.5194/gmd-2020-431
Preprint. Discussion started: 4 March 2021


Geoscientific Model Development Discussions

Kalnay, E., Kanamitsu, M., Kistler, R., Collins, W., Deaven, D., Gandin, L., Iredell, M., Saha, S., White, G., Woollen, J., Zhu, Y., Chelliah, M., Ebisuzaki, W., Higgins, W., Janowiak, J., Mo, K.C., Ropelewski, C., Wang, J., Leetmaa, A., Reynolds, R., Jenne, R., Joseph, D., 1996. The NCEP/NCAR 40-year reanalysis project. B Am Meteorol Soc 77, 437-471.

Kalvelage, T., Lavik, G., Jensen, M.M., Revsbech, N.P., Loscher, C., Schunck, H., Desai, D.K., Hauss, H., Kiko, R., Holtappels, M., LaRoche, J., Schmitz, R.A., Graco, M.I., Kuypers, M.M., 2015. Aerobic microbial respiration In oceanic oxygen minimum zones. PloS one 10.

Karstensen, J., Stramma, L., Visbeck, M., 2008. Oxygen minimum zones in the eastern tropical Atlantic and Pacific oceans. Progress in Oceanography 77, 331-350.

Keller, D.P., Kriest, I., Koeve, W., Oschlies, A., 2016. Southern Ocean biological impacts on global ocean oxygen. Geophysical Research Letters 43, 6469-6477.

Kessler, W.S., 2006. The circulation of the eastern tropical Pacific: A review. Progress in Oceanography 69, 181-217.

Kug, J.S., Kang, I.S., An, S.I., 2003. Symmetric and antisymmetric mass exchanges between the equatorial and off-equatorial Pacific associated with ENSO. Journal of Geophysical Research: Oceans 108.

Kuntz, L.B., Schrag, D.P., 2018. Hemispheric asymmetry in the ventilated thermocline of the Tropical Pacific. Journal of Climate 31, 1281-1288.

Levin, L.A., 2018. Manifestation, Drivers, and Emergence of Open Ocean Deoxygenation. Annual review of marine science 10, 229-260.

Libby, P.S., Wheeler, P.A., 1997. Particulate and dissolved organic nitrogen in the central and eastern equatorial Pacific. Deep-Sea Research Part I: Oceanographic Research Papers 44, 345-361.

Llanillo, P.J., Pelegri, J.L., Talley, L.D., Pena-Izquierdo, J., Cordero, R.R., 2018. Oxygen Pathways and Budget for the Eastern South Pacific Oxygen Minimum Zone. Journal of Geophysical Research: Oceans 123, 1722-1744.

Loginova, A.N., Thomsen, S., Dengler, M., Ludke, J., Engel, A., 2019. Diapycnal dissolved organic matter supply into the upper Peruvian oxycline. Biogeosciences 16, 2033-2047.

Murtugudde, R., Seager, R., Busalacchi, A., 1996. Simulation of the tropical oceans with an ocean GCM coupled to an atmospheric mixed-layer model. Journal of Climate 9, 1795-1815.

Oschlies, A., Brandt, P., Stramma, L., Schmidtko, S., 2018. Drivers and mechanisms of ocean deoxygenation. Nature Geoscience 11, 467-473.

Paulmier, A., Ruiz-Pino, D., 2009. Oxygen minimum zones (OMZs) in the modern ocean. Progress in Oceanography 80, 113-128.

Raimbault, P., Slawyk, G., Boudjellal, B., Coatanoan, C., Conan, P., Coste, B., Garcia, N., Moutin, T., Pujo-Pay, M., 1999. Carbon and nitrogen uptake and export in the equatorial Pacific at 150°W: Evidence of an efficient regenerated production cycle. Journal of Geophysical Research: Oceans 104, 3341-3356.

Schmidtko, S., Stramma, L., Visbeck, M., 2017. Decline in global oceanic oxygen content during the past five decades. Nature 542, 335-339.

Shigemitsu, M., Yamamoto, A., Oka, A., Yamanaka, Y., 2017. One possible uncertainty in CMIP5 projections of low-oxygen water volume in the Eastern Tropical Pacifi. Geophysical Research Letters 31, 804-820.

Sonnerup, R.E., Mecking, S., Bullister, J.L., 2013. Transit time distributions and oxygen utilization rates in the Northeast Pacific Ocean from chlorofluorocarbons and sulfur hexafluoride. Deep-Sea Res Pt I 72, 61-71.

Stramma, L., Johnson, G.C., Firing, E., Schmidtko, S., 2010. Eastern Pacific oxygen minimum zones: Supply paths and multidecadal changes. J Geophys Res-Oceans 115.

Stramma, L., Johnson, G.C., Sprintall, J., Mohrholz, V., 2008. Expanding oxygen-minimum zones in the tropical oceans. Science 320, 655-658.

Stramma, L., Oschlies, A., Schmidtko, S., 2012. Mismatch between observed and modeled trends in dissolved upper-ocean oxygen over the last 50 yr. Biogeosciences 9, 4045-4057.

Talley, L.D., Feely, R.A., Sloyan, B.M., Wanninkhof, R., Baringer, M.O., Bullister, J.L., Carlson, C.A., Doney, S.C., Fine, R.A., Firing, E., Gruber, N., Hansell, D.A., Ishii, M., Johnson, G.C., Katsumata, K., Key, R.M., Kramp, M., Langdon, C., Macdonald, A.M., Mathis, J.T., McDonagh, E.L., Mecking, S., Millero, F.J., Mordy, C.W., Nakano, T., Sabine, C.L., Smethie, W.M., Swift, J.H., Tanhua, T., Thurnherr, A.M., Warner, M.J., Zhang, J.Z., 2016. Changes in ocean heat, carbon content, and ventilation: a review of the first decade of go-ship global repeat hydrography. Annual review of marine science 8, 185-215.

https://doi.org/10.5194/gmd-2020-431
Preprint. Discussion started: 4 March 2021

Tiano, L., Garcia-Robledo, E., Dalsgaard, T., Devol, A.H., Ward, B.B., Ulloa, O., Canfield, D.E., Revsbech, N.P., 2014. Oxygen distribution and aerobic respiration in the north and south eastern tropical Pacific oxygen minimum zones. Deep-Sea Research Part I: Oceanographic Research Papers 94, 173-183.

Wang, X.J., Behrenfeld, M., Le Borgne, R., Murtugudde, R., Boss, E., 2009a. Regulation of phytoplankton carbon to chlorophyll ratio by light, nutrients and temperature in the Equatorial Pacific Ocean: a basin-scale model. Biogeosciences 6, 391-404.

Wang, X.J., Le Borgne, R., Murtugudde, R., Busalacchi, A.J., Behrenfeld, M., 2008. Spatial and temporal variations in dissolved and particulate organic nitrogen in the equatorial Pacific: biological and physical influences. Biogeosciences 5, 1705-1721.

Wang, X.J., Murtugudde, R., Hackert, E., Wang, J., Beauchamp, J., 2015. Seasonal to decadal variations of sea surface pCO2 and sea-air CO2 flux in the equatorial oceans over 1984–2013: A basin-scale comparison of the Pacific and Atlantic Oceans. Global Biogeochemical Cycles 29, 597-609.

Wang, X.J., Murtugudde, R., Le Borgne, R., 2009b. Nitrogen uptake and regeneration pathways in the equatorial Pacific: a basin scale modeling study. Biogeosciences 6, 2647-2660.

Wanninkhof, R., 1992. Relationship between wind speed and gas exchange over the Ocean. J Geophys Res-Oceans 97, 7373-7382.

Ward, B.A., Wilson, J.D., Death, R.M., Monteiro, F.M., Yool, A., Ridgwell, A., 2018. EcoGEnIE 1.0: plankton ecology in the cGEnIE Earth system model. Geoscientific Model Development 11, 4241-4267.

Weiss, R.F., 1970. The solubility of nitrogen, oxygen and argon in water and seawater. Deep-Sea Research 17, 721-735.

Williams, J.H.T., Totterdell, I.J., Halloran, P.R., Valdes, P.J., 2014. Numerical simulations of oceanic oxygen cycling in the FAMOUS Earth-System model: FAMOUS-ES, version 1.0. Geoscientific Model Development 7, 1419-1431.

https://doi.org/10.5194/gmd-2020-431
Preprint. Discussion started: 4 March 2021

Geoscientific Model Development Discussions

Tables

Table 1. Model experiments with different values for remineralization rate (C_{DON}) and vertical background diffusion (Kb).

Parameter	Unit	Reference	Cd0.5	Cd0.5 Kb0.1	Cd0.5 Kb0.3	Cd0.5 Kb0.5
C_{DON} (0-100 m)	d^{-1}	0.001	0.0005			
C_{DON} (100-600 m)		0.001-0.0005	0.0005-0.00025			
C_{DON} (600-1000 m)		0.0005	0.00025			
Kb	$cm^2 s^{-1}$	0	0	0.1	0.3	0.5

Table 2. Statistics for DO (mmol m^{-3}) comparisons between WOA2013 and model experiments over 1981-2000 in the Eastern Tropical North Pacific (ETNP) and Eastern Tropical South Pacific (ETSP).

Layers	Statistics	ETNP (165°W-90°W, 5°N-20°N)					ETSP (110°W-80°W, 10°S-3°S)				
		Reference	Cd0.5	Cd0.5 Kb0.1	Cd0.5 Kb0.3	Cd0.5 Kb0.5	Reference	Cd0.5	Cd0.5 Kb0.1	Cd0.5 Kb0.3	Cd0.5 Kb0.5
200-400 (m)	Bias	-9.45	-4.00	-3.96	-3.82	-3.60	-11.89	-3.59	-3.33	-2.67	-1.84
	MAE	15.17	15.70	15.56	15.27	14.98	11.89	3.72	3.55	3.15	3.12
	RMSE	19.01	17.34	17.18	16.82	16.44	12.18	4.44	4.28	3.92	3.57
400-700 (m)	Bias	-7.24	-4.99	-4.19	-2.49	-0.72	-10.36	-7.17	-5.79	-2.92	-0.04
	MAE	9.01	8.25	7.99	7.44	6.95	10.38	7.99	7.12	5.59	4.85
	RMSE	10.86	9.72	9.29	8.48	7.88	12.33	9.61	8.54	6.75	5.88
700-1000 (m)	Bias	-7.19	-4.49	-2.44	1.08	3.98	-12.90	-9.11	-6.48	-2.34	0.78
	MAE	7.18	4.67	4.12	4.17	5.28	13.33	10.42	8.81	6.98	6.47
	RMSE	9.22	6.85	5.49	4.67	5.92	16.14	12.81	10.79	8.33	7.59

Table 3. Comparisons of OMZ volume (10^{15} m^3) between WOA2013 and sensitivity experiments.

Regions	Waters	WOA2013	Reference	Cd0.5	Cd0.5 Kb0.1	Cd0.5 Kb0.3	Cd0.5 Kb0.5
North Pacific	Suboxic	5.97	10.47	8.87	8.29	7.36	6.61
	Hypoxic	19.98	21.21	20.48	20.35	20.01	19.62
South Pacific	Suboxic	1.43	3.49	2.42	2.20	1.85	1.56
	Hypoxic	7.12	9.90	8.73	8.35	7.70	7.13

Suboxic: DO <20 mmol m^{-3}; Hypoxic: DO <60 mmol m^{-3}.

https://doi.org/10.5194/gmd-2020-431
Preprint. Discussion started: 4 March 2021

Geoscientific Model Development Discussions

Figures

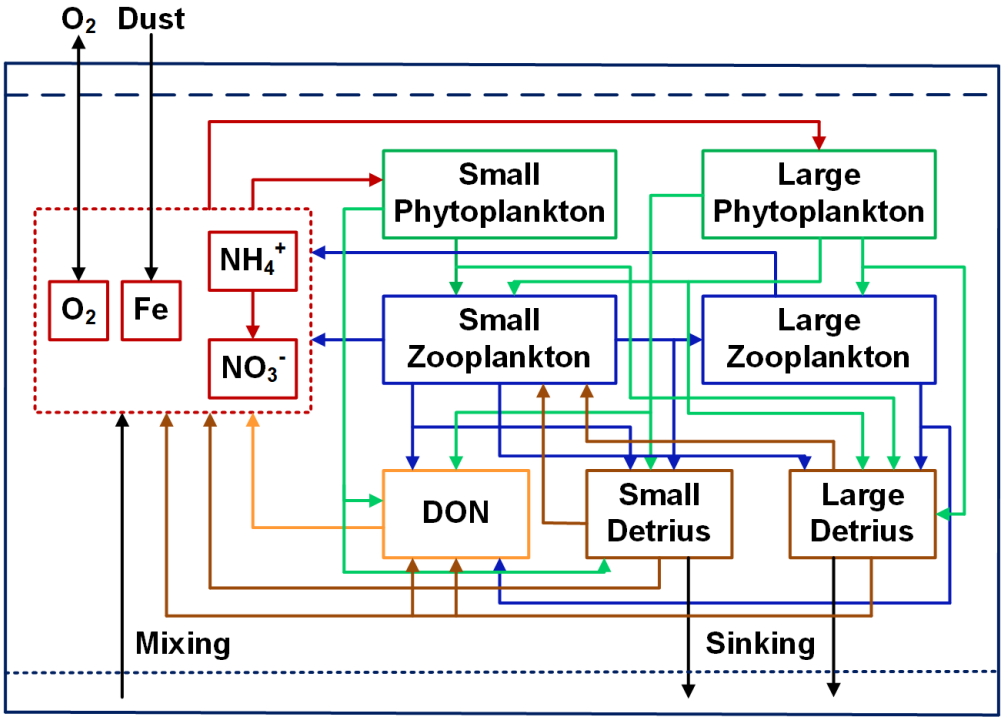

Figure 1. Flow diagram of ecosystem model. Red, green, blue, yellow and brown lines and arrows denote fluxes originating from inorganic forms, phytoplankton, zooplankton, DON and detritus, respectively.

https://doi.org/10.5194/gmd-2020-431
Preprint. Discussion started: 4 March 2021

Geoscientific Model Development Discussions

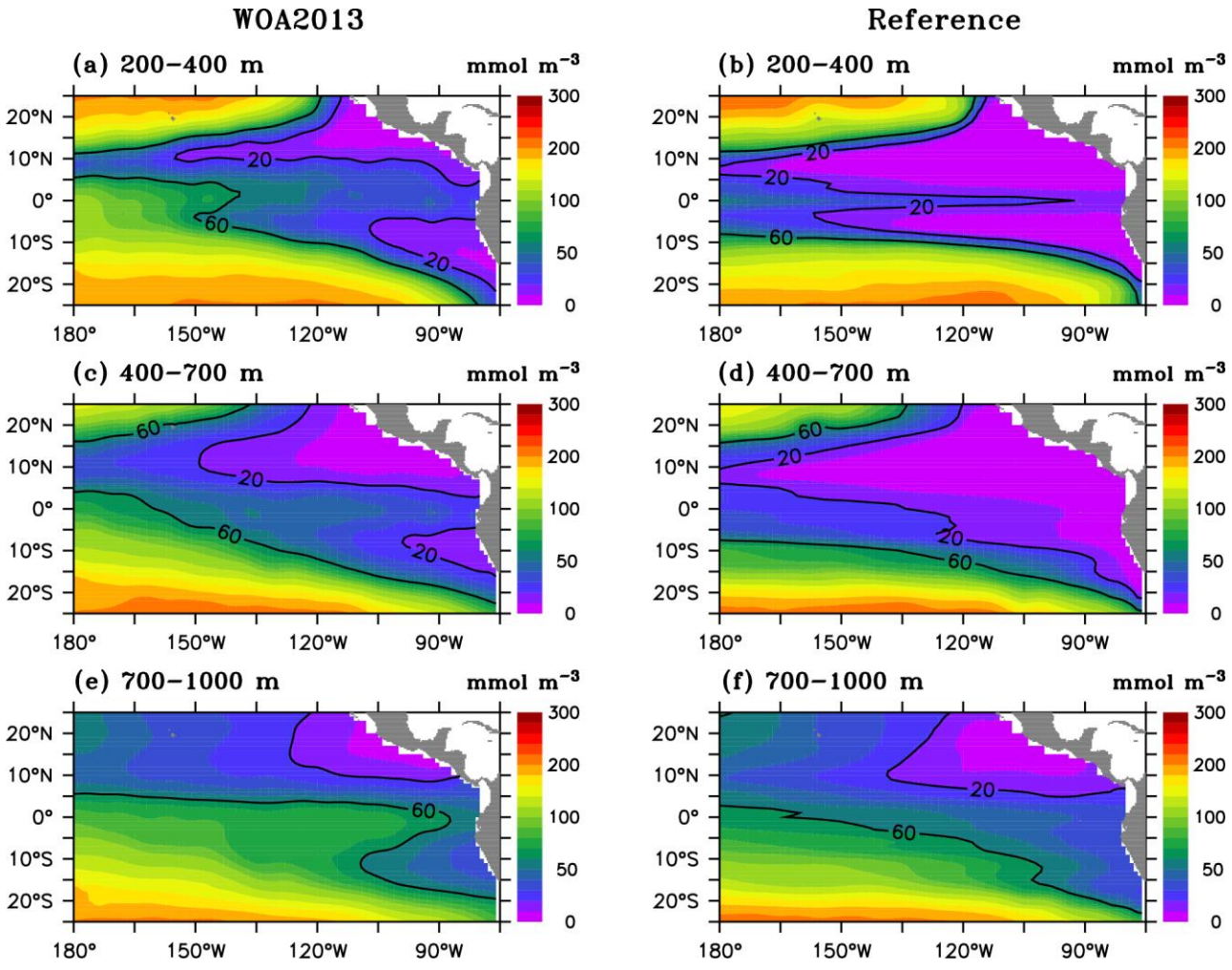

Figure 2. Comparisons of DO concentration between WOA2013 (left panel) and reference run during 1981-2000 (right panel).

https://doi.org/10.5194/gmd-2020-431
Preprint. Discussion started: 4 March 2021

Geoscientific Model Development Discussions

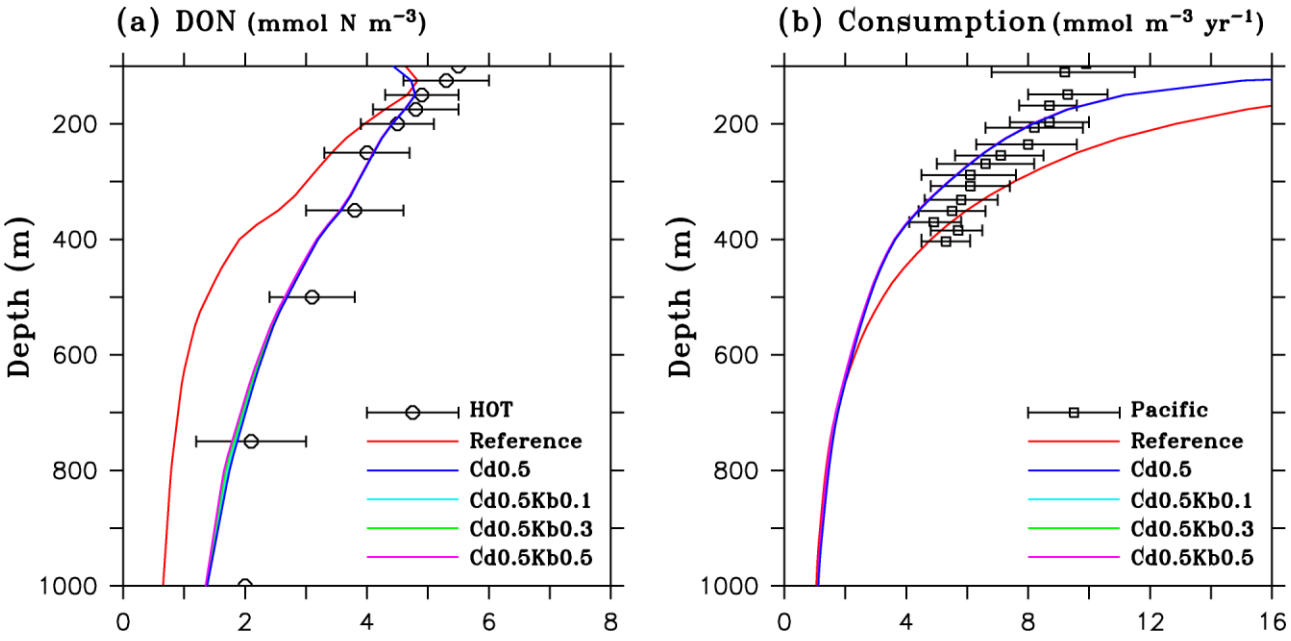

445 **Figure 3.** Comparisons of DON concentration **(a)** and consumption rate **(b)** between observation and model experiments. Observed DON data are from Hawaii Ocean Time-series program (HOT, 22°45'N, 158°00'W) (https://hahana.soest.hawaii.edu/hot/hot_jgofs.html). Observed consumption data are obtained from Karastensen et al., (2008) for the entire Pacific.

https://doi.org/10.5194/gmd-2020-431
Preprint. Discussion started: 4 March 2021

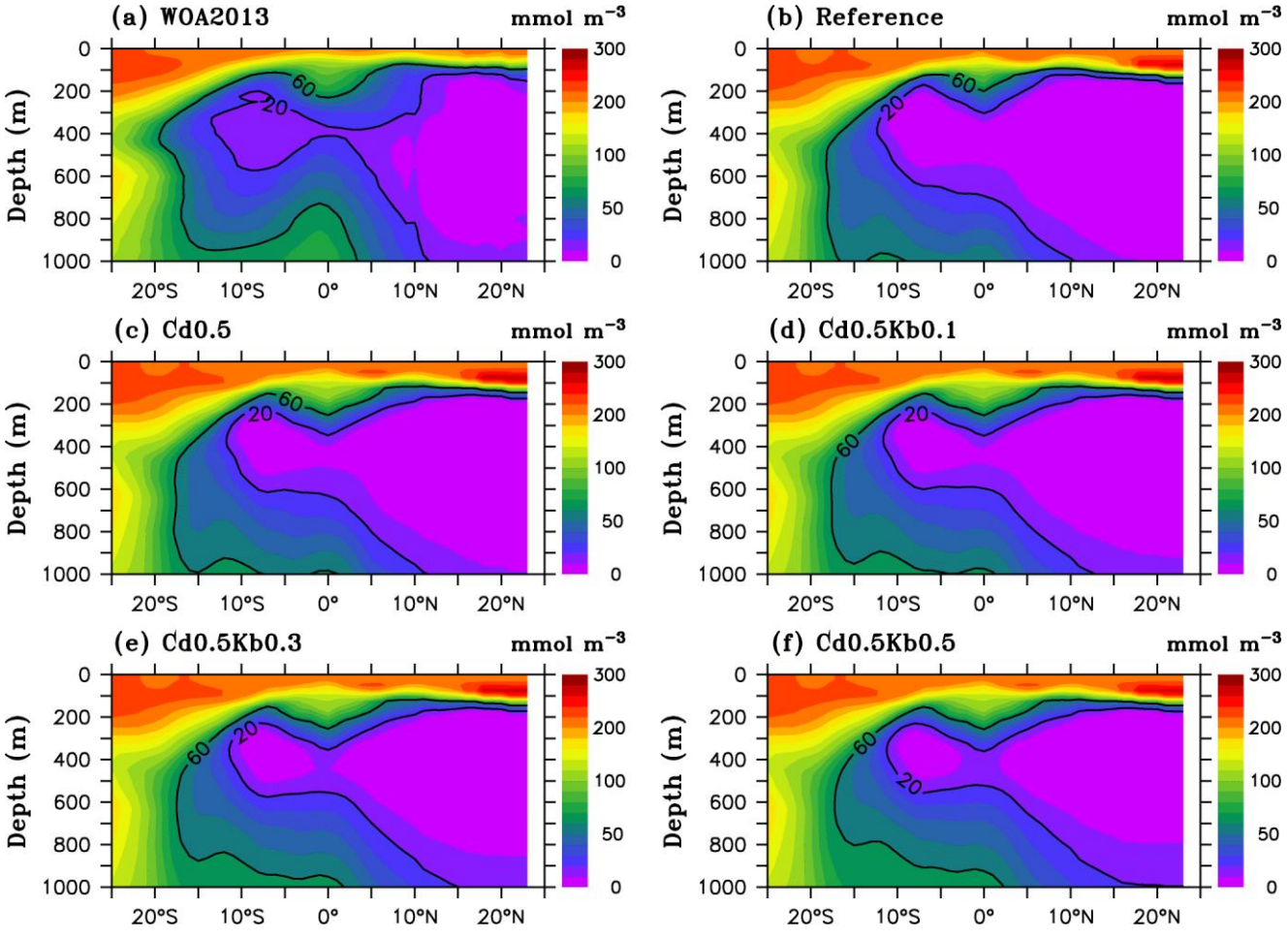

Figure 4. Observed and simulated DO from model experiments over 110°W-85°W. **(a)** WOA2013, **(b)** reference run, **(c)** Cd0.5, **(d)** Cd0.5Kb0.1, **(e)** Cd0.5Kb0.3, and **(f)** Cd0.5Kb0.5 over 1981-2000.

https://doi.org/10.5194/gmd-2020-431
Preprint. Discussion started: 4 March 2021

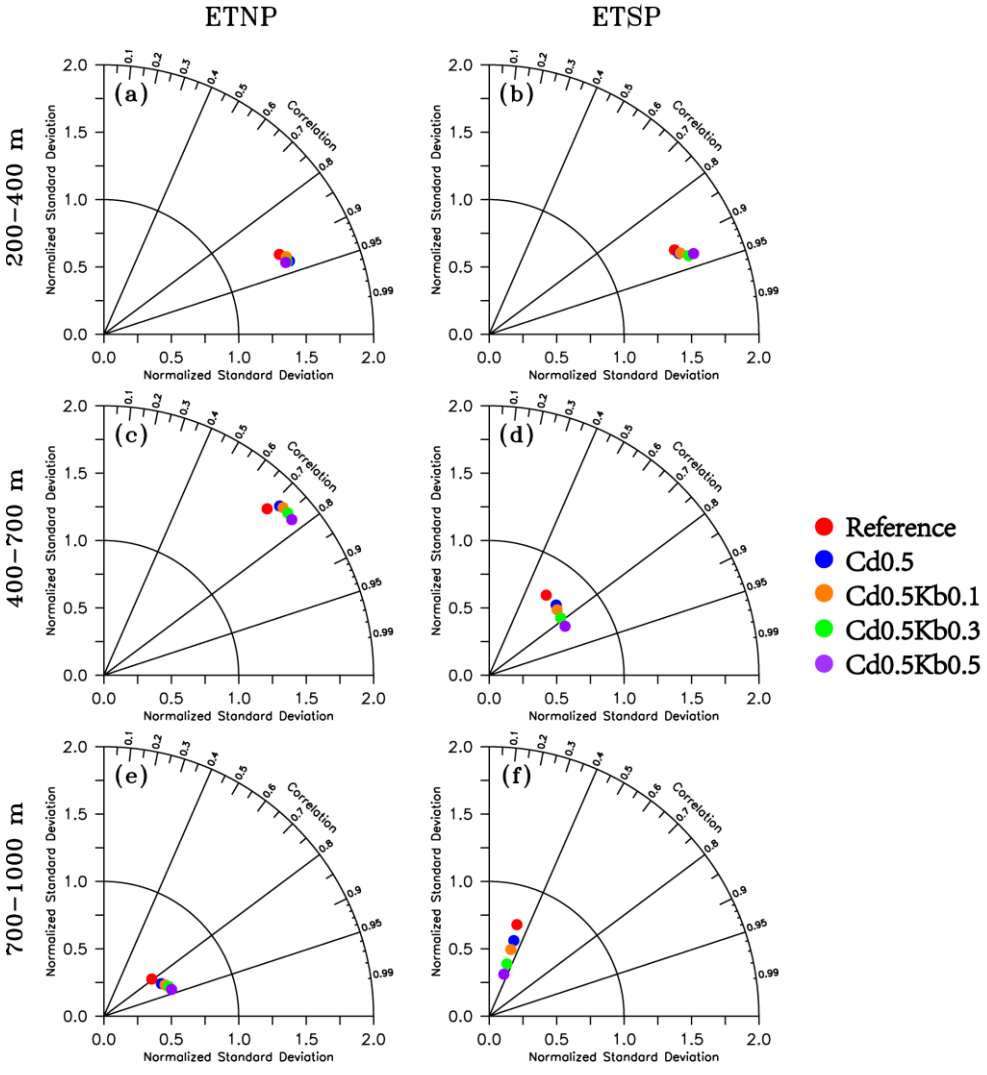

Figure 5. Taylor diagrams performed on the simulation of DO concentration between WOA2013 and model experiments for the left panel (ETNP: 165°W-90°W, 5°N-20°N) and right panel (ETSP: 110°W-80°W, 10°S-3°S) over 200-400 m, 400-700 m, and 700-1000 m.

https://doi.org/10.5194/gmd-2020-431
Preprint. Discussion started: 4 March 2021

Geoscientific Model Development Discussions

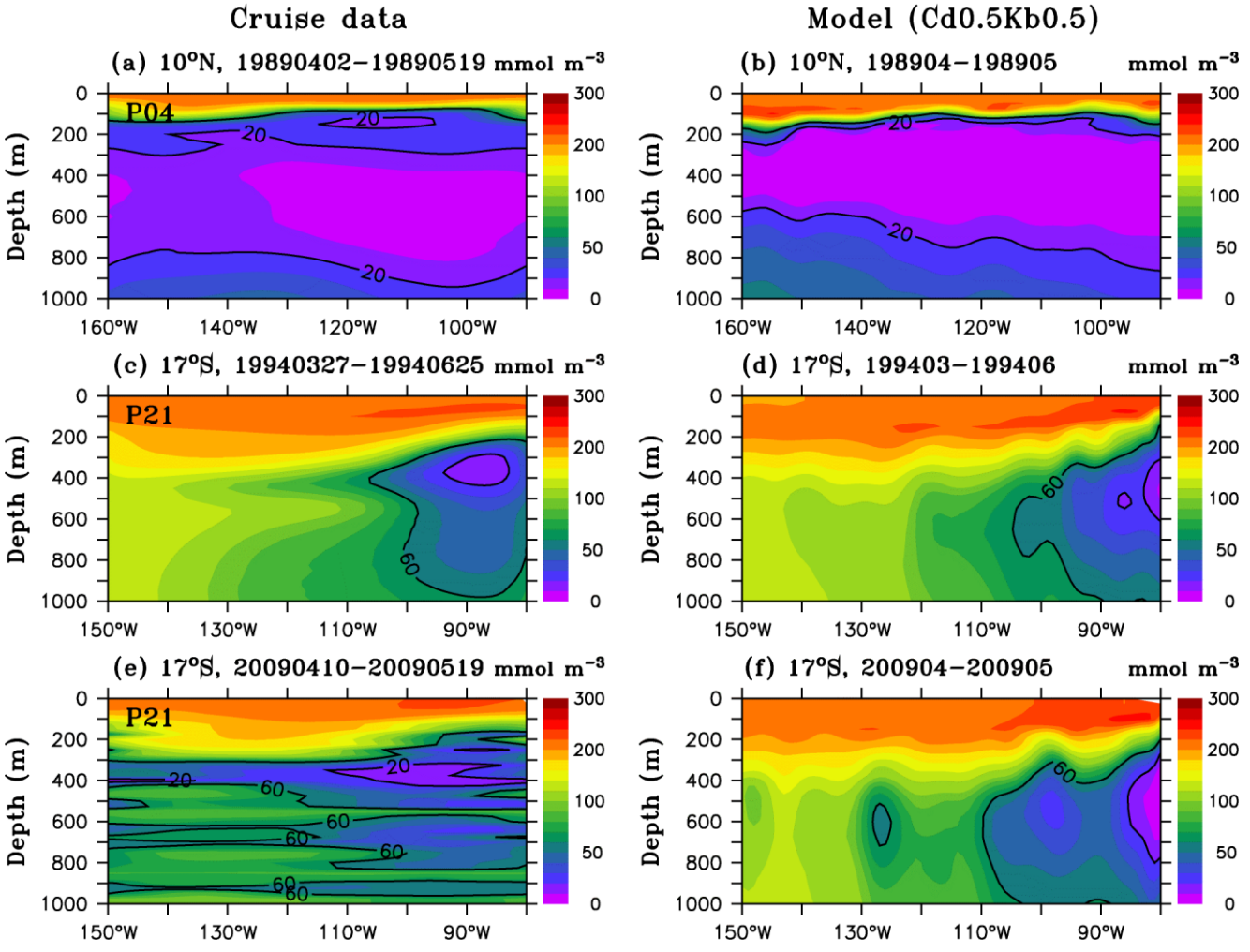

Figure 6. Distribution of DO from cruise data (left panel) and model results (right panel). Observed DO along the P04 and P21 lines are from CCHDO (https://cchdo.ucsd.edu/), which provides access to high quality global CTD and hydrographic data from GO-SHIP, WOCE, CLIVAR and other repeat hydrography programs.

https://doi.org/10.5194/gmd-2020-431
Preprint. Discussion started: 4 March 2021

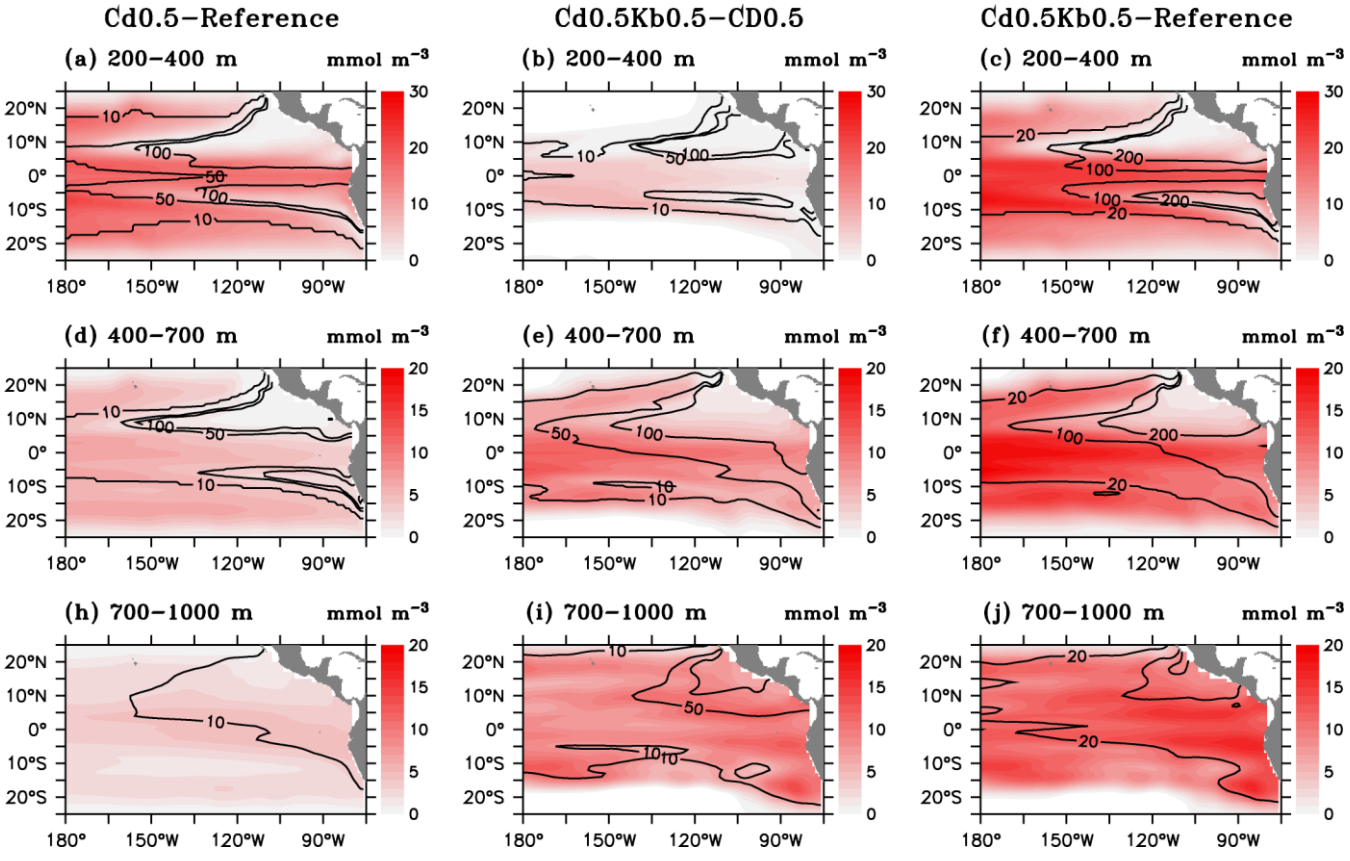

Figure 7. Changes of DO concentration due to reduced remineralization rate (left panel, Cd0.5 minus reference), enhanced mixing (middle panel, Cd0.5Kb0.5 minus Cd0.5), and their combination (right panel, Cd0.5Kb0.5 minus reference). Superimposed solid black lines denote the percentage of DO change relative to the reference run contoured by 10%, 50% and 100% in the left and middle panel, and 20%, 100% and 200% in the right panel.

https://doi.org/10.5194/gmd-2020-431
Preprint. Discussion started: 4 March 2021

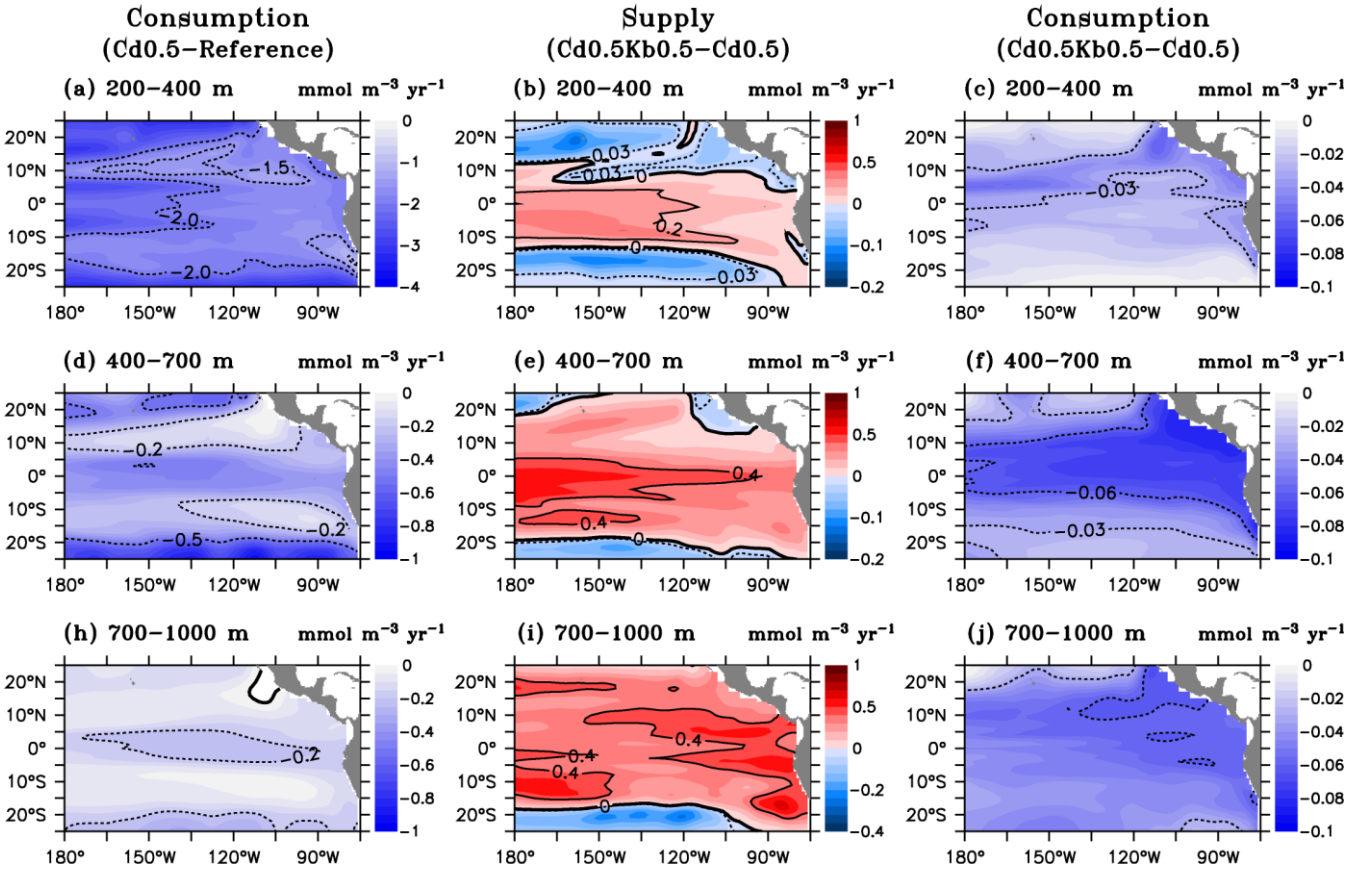

Figure 8. Decrease of DO consumption due to reduced remineralization rate (left panel, Cd0.5 minus reference), and changes in DO supply (middle panel, Cd0.5Kb0.5 minus Cd0.5) and decrease of DO consumption due to enhanced mixing (right panel, Cd0.5Kb0.5 minus Cd0.5).

https://doi.org/10.5194/gmd-2020-431
Preprint. Discussion started: 4 March 2021

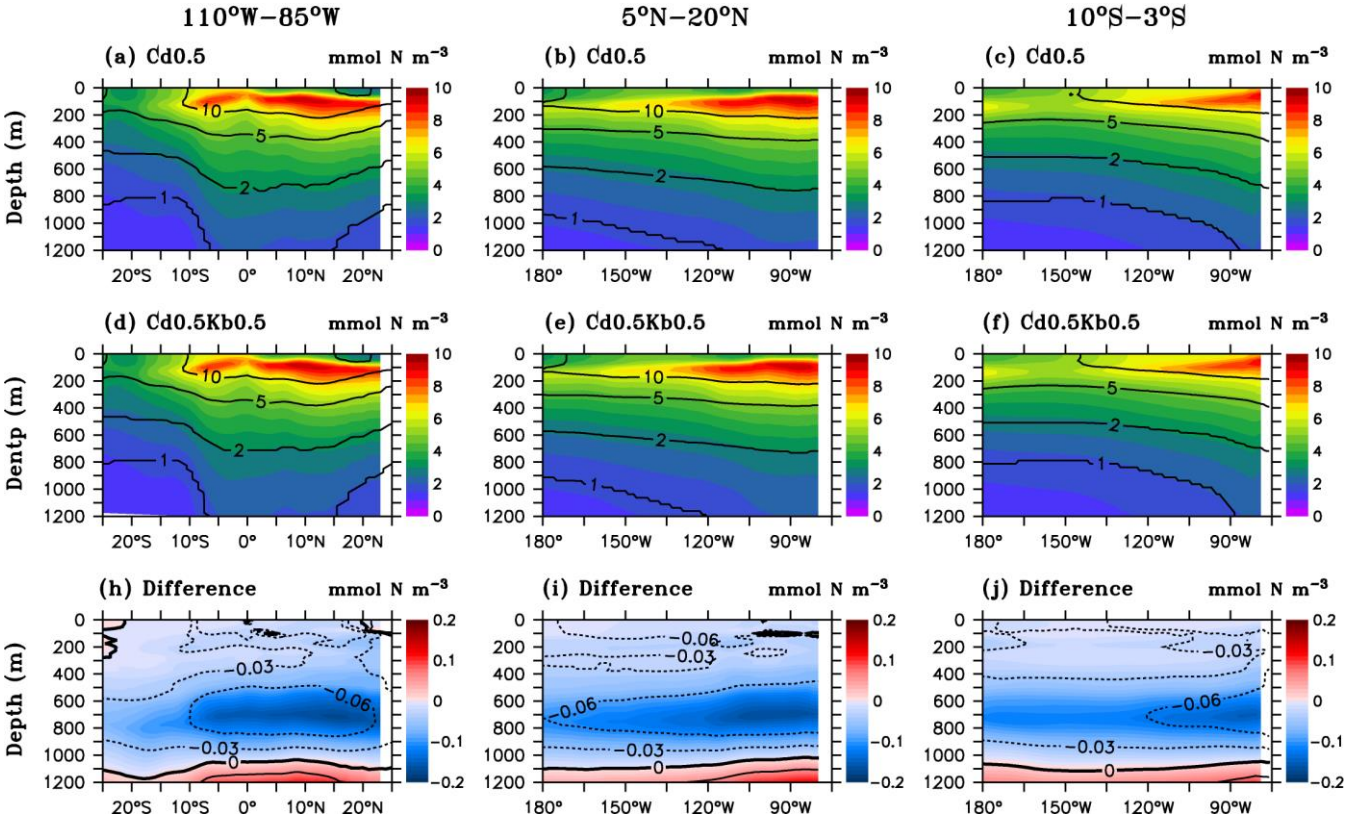

Figure 9. Distribution of DON and DON remineralization (mmol m^{-3} yr^{-1}) over 110°W-85°W (left panel), 5°N-20°N (middle panel), and 10°S-3°S (right panel) from **(a-c)** Cd0.5, **(d-f)** Cd0.5Kb0.5, and **(e-f)** their differences (Cd0.5Kb0.5 minus Cd0.5). Superimposed black lines denote consumption rate (mmol m^{-3} yr^{-1}) by remineralization of DON in **(a-f)** and the difference of consumption rate between Cd0.5Kb0.5 and Cd0.5 in **(h-j)**.

https://doi.org/10.5194/gmd-2020-431
Preprint. Discussion started: 4 March 2021

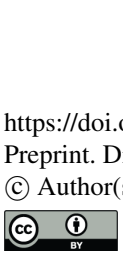

Geoscientific Model Development Discussions

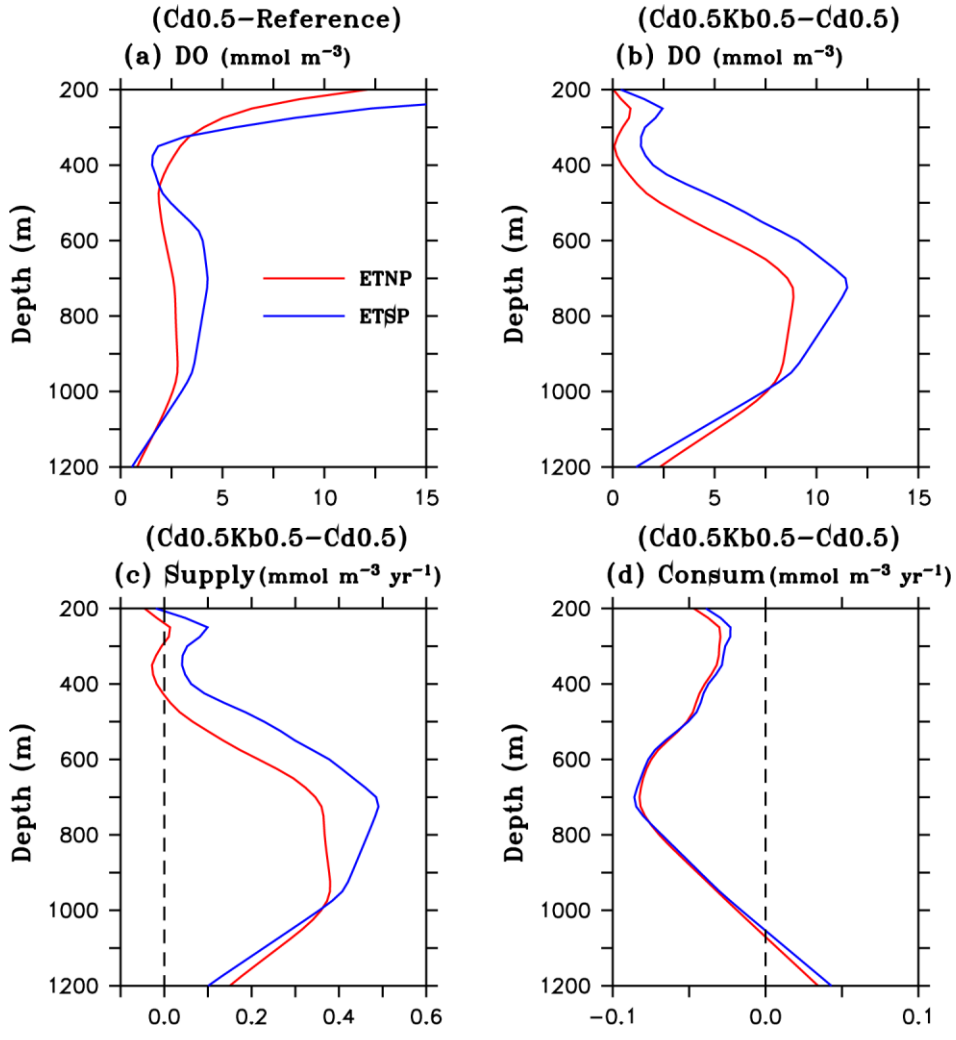

Figure 10. Changes due to reduced remineralization rate (Cd0.5 minus reference) for **(a)** DO, and enhanced mixing (Cd0.5Kb0.5 minus Cd0.5) for **(b)** DO, **(c)** physical supply, and **(d)** biological consumption. ETNP: 165°W-90°W, 5°N-20°N; ETSP: 110°W-80°W, 10°S-3°S.

https://doi.org/10.5194/gmd-2020-431
Preprint. Discussion started: 4 March 2021

Geoscientific Model Development Discussions

Appendix A

Model biogeochemical equations

Phytoplankton equations

$$\frac{\partial P_S}{\partial t} = \mu_S P_S - g_{P_S}(1 - e^{-\lambda P_S})Z_S - m_S P_S \quad \text{(B1)}$$

$$\frac{\partial P_L}{\partial t} = \mu_L P_L - g_{P_L1}(1 - e^{-\lambda P_L})Z_L - g_{P_L2}(1 - e^{-\lambda P_L})Z_S - m_L P_L \quad \text{(B2)}$$

Zooplankton equations

$$\frac{\partial Z_S}{\partial t} = [\lambda(g_{P_S}(1 - e^{-\lambda P_S}) + g_{P_L2}(1 - e^{-\lambda P_L})) + g_{D_S}(1 - e^{-\lambda D_S}) + g_{D_L2}(1 - e^{-\lambda D_L}) - (r_s + \delta_s)]Z_S - g_{Z_S}(1 - e^{-\lambda Z_S})\, Z_L \quad \text{(B3)}$$

$$\frac{\partial Z_L}{\partial t} = [\lambda(g_{P_L1}(1 - e^{-\lambda P_L}) + g_{Z_S}(1 - e^{-\lambda Z_S})) + g_{D_L1}(1 - e^{-\lambda D_L}) - (r_L + \delta_L)]Z_L \quad \text{(B4)}$$

Detritus equations

$$\frac{\partial D_S}{\partial t} = (m_S P_S + m_L P_L + (r_s Z_S + r_L Z_L)\chi)(1 - \gamma) - g_{D_S}(1 - e^{-\lambda D_S})Z_S - (c_{D_S} + \omega_{D_S} h^{-1})D_s \quad \text{(B5)}$$

$$\frac{\partial D_L}{\partial t} = (1 - \lambda)[\left(g_{P_S}(1 - e^{-\lambda P_S}) + g_{P_L2}(1 - e^{-\lambda P_L})\right)Z_S + \left(g_{P_L1}(1 - e^{-\lambda P_L}) + g_{Z_S}(1 - e^{-\lambda Z_S})\right)Z_L] + \delta_S Z_S + \delta_L Z_L - (c_{D_L} + \omega_{DL} h^{-1})D_L - g_{D_L2}(1 - e^{-\lambda D_L})Z_S - g_{D_L1}(1 - e^{-\lambda D_L})Z_L \quad \text{(B6)}$$

DON equations

$$\frac{\partial DON}{\partial t} = (m_S P_S + m_L P_L + (r_s Z_S + r_L Z_L)\chi)\gamma + (c_{D_S} D_S + c_{D_L} D_L)\zeta - c_{DON} DON \quad \text{(B7)}$$

Nutrients equations

$$\frac{\partial \mathrm{NO_3}}{\partial t} = -\mu_S P_S \frac{N_{S\_UP}}{N_{S\_UP} + A_{UP}} - \mu_L P_L \frac{N_{L\_UP}}{N_{L\_UP} + A_{UP}} + \varphi NH_4 \quad \text{(B8)}$$

$$\frac{\partial \mathrm{NH_4}}{\partial t} = -\mu_S P_S \frac{A_{up}}{N_{S\_UP} + A_{UP}} - \mu_L P_L \frac{A_{up}}{N_{L\_UP} + A_{UP}} + (r_S Z_S + r_L Z_L)(1 - \chi) + c_{DON} DON + (c_{D_S} D_S + c_{D_L} D_L)(1 - \zeta) - \varphi NH_4 \quad \text{(B9)}$$

$$\frac{\partial \mathrm{Fe}}{\partial t} = -(\mu_S P_S R_S + \mu_L P_L R_L - s_{Fe} D_L Fe) + R_S[(r_S Z_S + r_L Z_L)(1 - \chi) + c_{DON} DON + c_{D_S} D_S + c_{D_L} D_L(1 - \zeta)] \quad \text{(B10)}$$

Nitrogen uptake

$$N_{S\_UP} = \frac{NO_3}{K_{S\_NO_3} + NO_3}\left(1 - \frac{NH_4}{K_{NH_4} + NH_4}\right) \quad \text{(B11)}$$

$$N_{L\_UP} = \frac{NO_3}{K_{L\_NO_3} + NO_3}\left(1 - \frac{NH_4}{K_{NH_4} + NH_4}\right) \quad \text{(B12)}$$

https://doi.org/10.5194/gmd-2020-431
Preprint. Discussion started: 4 March 2021


Geoscientific Model Development Discussions

$$A_{UP} = \frac{NH_4}{K_{NH_4}+NH_4} \quad \text{(B13)}$$

525

Other equations

Phytoplankton growth rate

$$\mu_S = \mu_{S0} e^{k_T T} f(I) \psi_S(N, Fe) \quad \text{(B14)}$$

530 $$\mu_L = \mu_{L0} e^{k_T T} f(I) \psi_L(N, Fe) \quad \text{(B15)}$$

Nutrient limitation

$$\psi_S(N, Fe) = \min\left(\frac{NO_3+NH_4}{K_{S\_N}+NO_3+NH_4}, \frac{\mathrm{Fe}}{K_{S\_\mathrm{Fe}}+\mathrm{Fe}}\right) \quad \text{(B16)}$$

$$\psi_L(N, Fe) = \min\left(\frac{NO_3+NH_4}{K_{L\_N}+NO_3+NH_4}, \frac{\mathrm{Fe}}{K_{L\_\mathrm{Fe}}+\mathrm{Fe}}\right) \quad \text{(B17)}$$

535

Light limitation

$$f(I) = 1 - e^{-\frac{\alpha I}{\eta P_{MAX}}} \quad \text{(B18)}$$

Light attenuation

540 $$I(z) = I_0 exp^{-k_A Z} \quad \text{(B19)}$$

$$k_A = k_W + k_C \mathrm{Chl} + k_D(D_S+D_L) \quad \text{(B20)}$$

Detritus decomposition and DON remineralization

$$c_{DS} = c_{DS0} e^{k_B(T-10)} \quad \text{(B21)}$$

545 $$c_{DL} = c_{DL0} e^{k_B(T-10)} \quad \text{(B22)}$$

$$c_{DON} = c_{DON0} e^{k_B(T-10)} \quad \text{(B23)}$$

Phytoplankton carbon to chlorophyll ratio (η)

$$\mathrm{Chl} = \left(\frac{P_S}{\eta_S} + \frac{P_L}{\eta_L}\right) R_{C:N} \quad \text{(B24)}$$

550 $$\eta_S = \eta_{S0} - (\eta_{S0} - \eta_{MIN}) \frac{lnI_0 - lnI}{4.605} \quad \text{(B25)}$$

$$\eta_L = \eta_{L0} - (\eta_{L0} - \eta_{MIN}) \frac{lnI_0 - lnI}{4.605} \quad \text{(B26)}$$

$$\eta_{S0} = \eta_{S\_MAX} - k_{PS} \mu_S^* \quad \text{(B27)}$$

$$\eta_{L0} = \eta_{L\_MAX} - k_{PL} \mu_L^* \quad \text{(B28)}$$

https://doi.org/10.5194/gmd-2020-431
Preprint. Discussion started: 4 March 2021

Geoscientific Model Development Discussions

$$\mu_S^* = \mu_{S0} e^{k_T T} \min\left(\frac{NO_3}{K_{S\_N}+NO_3}, \frac{\mathrm{Fe}}{K_{S\_\mathrm{Fe}}+\mathrm{Fe}}\right) \quad \text{(B29)}$$

$$\mu_L^* = \mu_{L0} e^{k_T T} \min\left(\frac{NO_3}{K_{L\_N}+NO_3}, \frac{\mathrm{Fe}}{K_{L\_\mathrm{Fe}}+\mathrm{Fe}}\right) \quad \text{(B30)}$$

https://doi.org/10.5194/gmd-2020-431
Preprint. Discussion started: 4 March 2021

Geoscientific Model Development Discussions

Appendix B

Model biogeochemical parameters

Symbol	Parameter	Unit	Value
m_S	Small phytoplankton mortality rate	d^{-1}	0.15
m_L	Large phytoplankton mortality rate	d^{-1}	0.35
r_S	Small zooplankton excretion rate	d^{-1}	0.53
r_L	Large zooplankton excretion rate	d^{-1}	0.44
δ_S	Small zootoplankton mortality rate	d^{-1}	0.12
δ_L	Large zootoplankton mortality rate	d^{-1}	0.12
g_{Ps}	Maximum grazing rate for small phytoplanktion	d^{-1}	2.6
g_{PL1}	Maximum grazing rate for large phytoplanktion	d^{-1}	1.2
g_{Zs}	Maximum grazing rate for small zootoplanktion	d^{-1}	1.7
g_{PL2}	Maximum grazing rate for large phytoplanktion	d^{-1}	0.9
g_{Ds}	Maximum grazing rate for small detritus	d^{-1}	1.0
g_{DL1}	Maximum grazing rate for large detritus	d^{-1}	3.0
g_{DL2}	Maximum grazing rate for large detritus	d^{-1}	1.5
Λ	Ivlev coefficient	$(mmol\ m^{-3})^{-1}$	0.5
λ	Zootoplankton assimilation coefficient	%	75
χ	Excretion coefficient	%	55
γ	Dissolution coefficient	%	90
ξ	Dissolution coefficient	%	90
$R_{C:N}$	C:N ratio	mol:mol	6.625
R_S	Fe:N ratio for small phytoplankton	μmol:mol	15
R_L	Fe:N ratio for large phytoplankton	μmol:mol	40
η_{S_MIN}	Minimum PhyC:Chl ratio in small phytoplanktion	g:g	30
η_{L_MIN}	Minimum PhyC:Chl ratio in large phytoplanktion	g:g	15
η_{S_MAX}	Maximum PhyC:Chl ratio in small phytoplanktion	g:g	200
η_{L_MAX}	Maximum PhyC:Chl ratio in large phytoplanktion	g:g	120
k_{Ps}	Photoacclimation coefficient for small phytoplanktion	(g:g)d	95

https://doi.org/10.5194/gmd-2020-431
Preprint. Discussion started: 4 March 2021

Geoscientific Model Development Discussions

k_{PL}	Photoacclimation coefficient for large phytoplanktion	(g:g)d	70
w_{DS}	Sinking velocity for small detritus	m d^{-1}	1
w_{DL}	Sinking velocity for large detritus	m d^{-1}	3.5
φ	Nitrification rate (when I<5 μmolEm^{-2} s^{-1})	d^{-1}	0.04
s_{Fe}	Iron scavenge coefficient	d^{-1} (nmol Fe m^{-3})$^{-1}$	0.00001
μ_{S0}	Maximum growth rate at 0°C for small phytoplankton	d^{-1}	0.58
μ_{L0}	Maximum growth rate at 0°C for large phytoplankton	d^{-1}	1.16
k_T	Temp. Dependent coefficient for μ	$°C^{-1}$	0.06
K_{S_N}	Half saturation constant for N limitation	mmol m^{-3}	0.3
K_{L_N}	Half saturation constant for N limitation	mmol m^{-3}	0.9
K_{S_Fe}	Half saturation constant for iron limitation	mmol m^{-3}	14
K_{L_Fe}	Half saturation constant for iron limitation	mmol m^{-3}	150
K_{S_NO3}	Half saturation constant for nitrate uptake	mmol m^{-3}	0.3
K_{L_NO3}	Half saturation constant for nitrate uptake	mmol m^{-3}	0.9
K_{NH4}	Half saturation constant for ammonium uptake	mmol m^{-3}	0.05
α	Initial slope of the P – I curve	mg C mg chl^{-1}(μmol E m^{-2} s^{-1})$^{-1}$	0.02
P_{MAX}	Maximum carbon specific growth rate	h^{-1}	0.036
k_W	Light attenuation constant for water	m^{-1}	0.028
k_C	Light attenuation constant for chlorophyll	m^{-1} (mg chl $m^{-3)-1}$	0.058
k_D	Light attenuation constant for detritus	m^{-1} (mg chl $m^{-3)-1}$	0.008
c_{DS0}	Small detritus decomposition rate at 10°C	d^{-1}	0.001
c_{DL0}	Large detritus decomposition rate at 10°C	d^{-1}	0.008
c_{DON0}	DON remineraization rate (0-100 m) at 10°C	d^{-1}	0.001
	100-500 m at 10°C	d^{-1}	0.0002-0.001
	>500 m at 10°C	d^{-1}	0.0002
k_B	Temp. dependent coefficient for c	$°C^{-1}$	0.02